Electronic Supplementary Information

A Magnetic Look into the Protecting Layer of Au_{25} Clusters

Mikhail Agrachev, Sabrina Antonello, Tiziano Dainese, José A. Gascón, Fangfang Pan, Kari Rissanen, Marco Ruzzi, Alfonso Venzo, Alfonso Zoleo, and Flavio Maran

Table of Contents:

1. Chemicals. Hydrogen tetrachloroaurate trihydrate (Aldrich, 99.9%), tetra-*n*-octylammonium bromide (Aldrich, 98%), ethanethiol (Aldrich, 97%), sodium borohydride (Aldrich, 99%), tetrahydrofuran (THF, Sigma-Aldrich, 99.9%), toluene (Sigma-Aldrich, 99.7%), diethyl ether (Sigma-Aldrich, 99.8%), acetonitrile-d_3 (Aldrich, 99.8%, d_3), benzene-d_6 (Aldrich, 99.6%, d_6), and *trans*-2-[3-(4-*tert*-butylphenyl)-2-methyl-2-propenylidene] malononitrile (DCTB, Sigma-Aldrich, ≥98%) were used as received. For electrochemistry, dichloromethane (DCM, VWR, 99.8%) was freshly distilled over CaH2 and stored under an argon atmosphere. Tetra-*n*-butylammonium hexafluorophosphate (Fluka, 99%) was recrystallized from ethanol. Low conductivity water was milliQ Water pro analysis (Merck). Column chromatography was carried out using silica gel from Macherey-Nagel (MN-Kieselgel 60 M, 230-400 mesh).

MALDI-TOF experiments were carried out with an Applied Biosystems 4800 MALDI-TOF/TOF spectrometer equipped with a Nd:YAG laser operating at 355 nm. The laser-firing rate was 200 Hz and the accelerating voltage was 25 kV. DCTB was used as the matrix. The clusters were dissolved in dichoromethane containing DCTB to obtain 0.1 mM solutions with a 1:400 MPC/matrix ratio. 2 μl of solution were dropcasted onto the sample plate and air-dried before loading into MALDI-TOF. The spectra were recorded using the reflectron positive- or negative-ion mode.

2. Synthesis of $Au_{25}(SPr)_{18}$. 0.50 g (1.27 mmol) of $HAuCl_4 \cdot 3H_2O$ was dissolved in 40 ml THF and then 0.833 g of tetra-*n*-octylammonium bromide (1.52 mmol, 1.2 equiv) were added to form a red solution. After stirring for 15 min at room temperature at moderate speed, magnetic stirring was increased to 100 rpm and then 0.460 ml (5.08 mmol, 4 equiv) of 1-propanethiol in 10 ml of THF was added dropwise. The resulting yellow solution became colorless in ca. 30 min. Magnetic stirring was increased to 600 rpm and a freshly prepared icy-cold aqueous solution (10 ml) of $NaBH_4$ (0.48 g, 12.7 mmol, 10 equiv) was added and this caused the resulting mixture to become black. After two days, the reaction mixture was filtered on paper and THF was evaporated to leave a reddish-brown oily solid covered by residual H_2O from aq. $NaBH_4$. The water phase was

removed, and the solid was dissolved in toluene and washed with water (4 x 40 ml) in a separatory funnel. Toluene was evaporated, the solid was dissolved in 50 ml of DCM, and the resulting solution was left to rest overnight in the dark at 4°C. The white residue precipitated during this treatment was discarded and DCM was then evaporated. The resulting oily solid was further purified by dissolving it in a mixture of diethyl ether and pentane to precipitate most of the residual tetraoctylammonium salt. The last traces of salt were eliminated by washing the product a few times with icy-cold methanol. The final product, $[n\text{-}Oct_4N^+][Au_{25}(SPr)_{18}^-]$, is a dark-orange brown powder. For the NMR spectroscopy measurements, possible traces of the oxidized cluster, which could form by air oxidation during the methanol washes, were eliminated by rinsing the product a few times with pentane.

Oxidation of the as-prepared cluster to obtain the paramagnetic species $Au_{25}(SPr)_{18}^0$ was performed by a passage through a silica-gel chromatography column, using DCM as eluent and compressed air as the pushing gas. Upon injection of the orange solution of the anionic cluster in DCM into the column, the solution turned green while passing through the column. After evaporation of the solvent, the oxidized cluster appeared as a black-brownish powder. The cluster was further purified by washing thrice with acetonitrile, in which $Au_{25}(SPr)_{18}^0$ is insoluble. The resulting neutral cluster $Au_{25}(SPr)_{18}^0$ had the typical UV-vis behavior distinctly different from that of the corresponding anion, as already described for, *e.g.*, $Au_{25}(SEt)_{18}$.[S1] The expected molecular mass was observed by using matrix-assisted laser desorption ionization time-of-flight (MALDI-TOF) mass spectrometry (Figure S1).

$Au_{25}(SPr)_{18}^0$ was recrystallized by adding a drop of acetonitrile to a concentrated solution of the cluster in 1:2 toluene-pentane and leaving the solvents to evaporate for some days in the dark at room temperature. Its structure was resolved by X-ray diffraction, as described in the next section **7**.

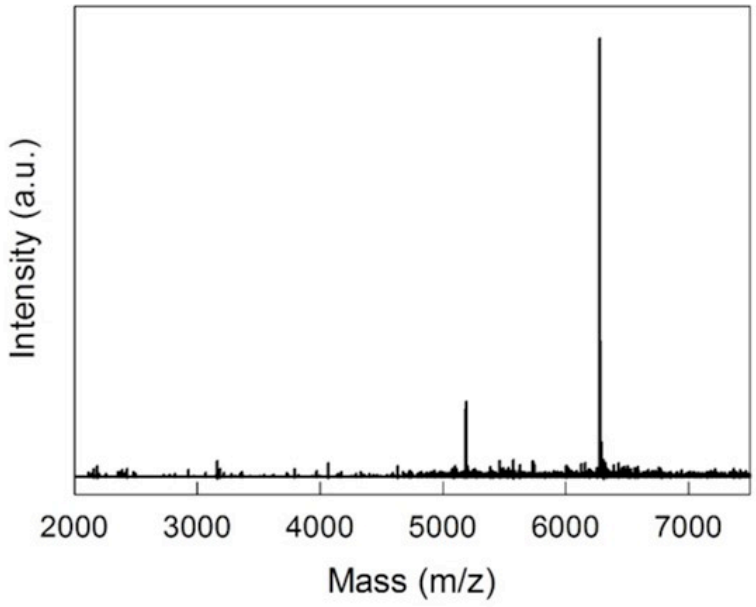

Figure S1. Positive-mode MALDI-TOF spectrum of $Au_{25}(SPr)_{18}^{0}$. The peak at 5188.48 corresponds to the fragmentation product $Au_{21}(SPr)_{14}$.

3. Synthesis of $Au_{25}(SMePr)_{18}$. $Au_{25}(SMePr)_{18}$ was synthesized, purified, oxidized, and characterized, for both charge states, as already described in detail for $Au_{25}(SPr)_{18}$. Figures S2-S4 show the ^{1}H NMR spectra of 2-methyl-propanethiol and two charge states of the cluster, in benzene-d_6.

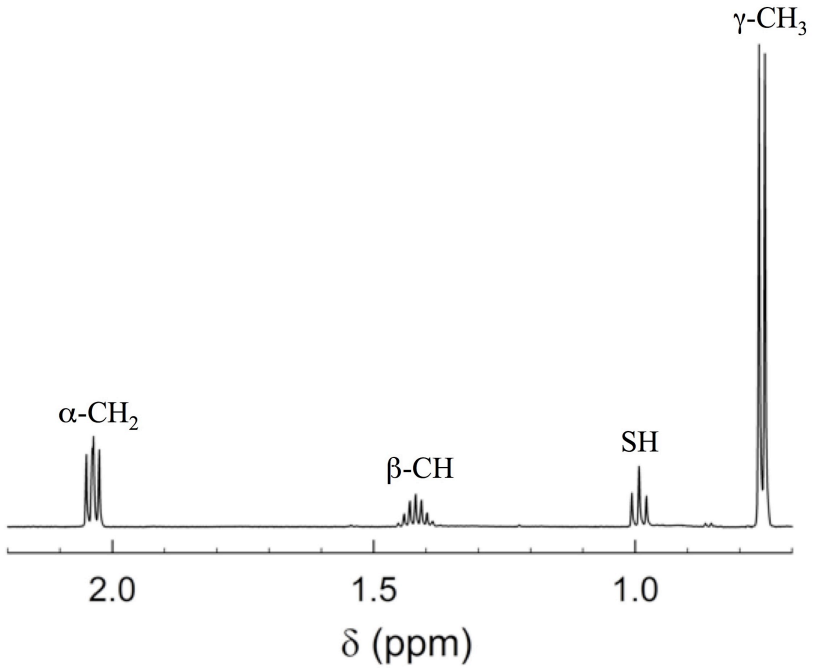

Figure S2. ^{1}H NMR spectrum of 2-methyl-propanethiol at 25°C.

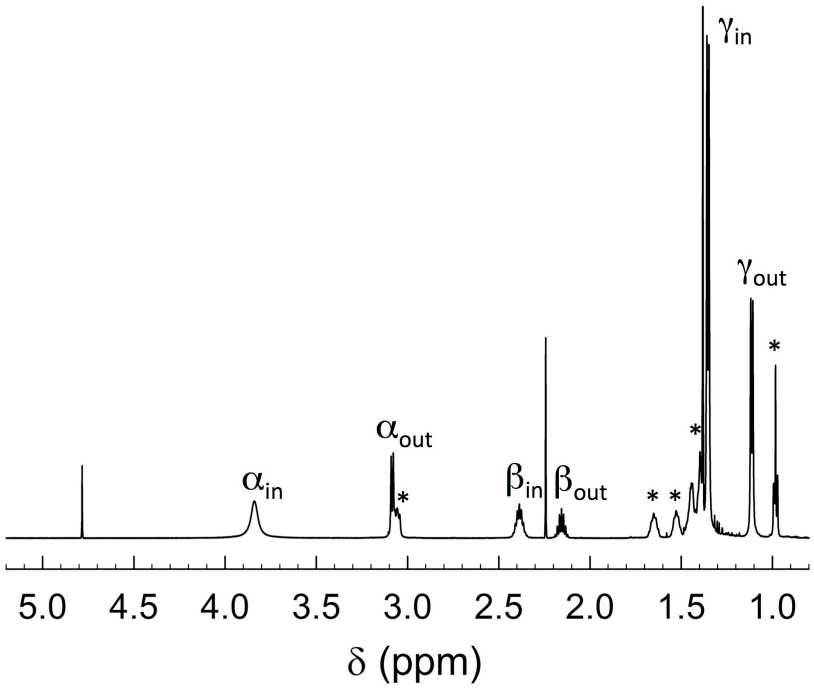

Figure S3. ^{1}H NMR spectrum of 3 mM [*n*-Oct_4N^+][$Au_{25}(SMePr)_{18}^-$] at 25°C. The asterisks mark the *n*-Oct_4^+ cation.

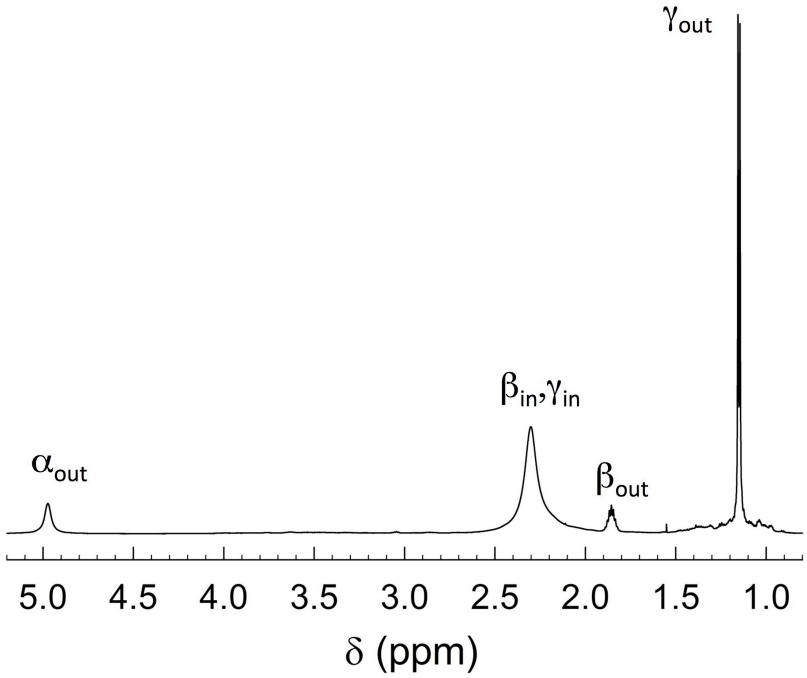

Figure S4. ^{1}H NMR spectrum of 3 mM $Au_{25}(SMePr)_{18}^{0}$ at 25°C. The overlapping β_{in} and γ_{in} resonances split at higher temperatures.

4. ^{1}H and ^{13}C NMR Spectroscopy Data. The following NMR spectroscopy data (δ) were obtained in benzene-d_6 at 298 K. For the four anionic clusters, the ^{1}H NMR signals pertaining to the tetra-*n*-octylammonium cation, *n*-Oct_4N^+, are found at: 3.09 (8H, 4 NCH_2), 1.55, 1.45, 1.40, 1.39, 1.37 and 1.41 (48H, 4 x 6CH_2), 0.98 (12H, 4CH_3). As already observed,[S2] the ^{13}C NMR signals for the α_{in} and β_{in} resonances occur at very large absolute δ values whose determination would require exceedingly long acquisition times, which goes beyond the scope of the present investigation.

$Au_{25}(SEt)_{18}$

[*n*-Oct_4N^+][$Au_{25}(SEt)_{18}^-$].^{1}H NMR: : 3.879 (q, 24H, α_{in}), 3.139 (q, 12H, α_{out}), 1.710 (t, 36H, β_{in}), 1.362 (t, 18H, β_{out}). ^{13}C NMR: 33.0 (12C, α_{in}), 28.6 (6C, α_{out}), 21.8 (12C, β_{in}), 19.5 (6C, β_{out}).

$Au_{25}(SEt)_{18}^{0}$.^{1}H NMR: 25.4 (very br s, 24H, α_{in}), 4.900 (br s, 12H, α_{out}), 4.121(br s, 36H, β_{in}), 1.19 (t, 18H, β_{out}). ^{13}C NMR: 35.5 (6C, α_{out}), 27.9 (6C, β_{out}).

$Au_{25}(SPr)_{18}$

[*n*-Oct_4N^+][$Au_{25}(SPr)_{18}^-$]. ^{1}H NMR: 3.885 (t, 24H, α_{in}), 3.15 (t, 12H, α_{out}), 2.213 (sextet, 24H, β_{in}), 1.894 (sext, 12H, β_{out}), 1.227 (t, 36H, γ_{in}), 0.980 (t, 18H, γ_{out}). ^{13}C NMR: 40.23 (12C, α_{in}), 36.18 (6C, α_{out}), 30.15 (12C, β_{in}), 28.36 (6C, β_{out}), 14.39 (6C, γ_{out}), and 13.90 (12C, γ_{in}).

$Au_{25}(SPr)_{18}^0$. ^{1}H NMR: 25.0 (very br s, 24H, α_{in}), 4.924 (br s, 12H, α_{out}), 3.381 (br s, 24H, β_{in}), 2.132 (br t, 36H, γ_{in}), 1.689 (sext, 12H, β_{out}), 1.019 (t, 18H, γ_{out}). ^{13}C NMR: 40.22 (6C, α_{out}), 36.22 (6C, β_{out}), 23.08 (12C, γ_{in}) and 14.39 (6C, γ_{out}).

$Au_{25}(SBu)_{18}$

[*n*-Oct_4N^+][$Au_{25}(SBu)_{18}^-$]. ^{1}H NMR: 3.933 (t, 24H, α_{in}), 3.226 (t, 12H, α_{out}), 2.207 (m, 24H, β_{in}), 1.912 (m, 12H, β_{out}), 1.732 (m, 24H, γ_{in}), 1.485 (m, 12H, γ_{out}), 1.072 (t, 36H, δ_{in}), 0.881 (t, 18H, δ_{out}). ^{13}C NMR: 29.24 (12C, α_{in}), 38.92 (6C, α_{out}), 40.98 (12C, β_{in}), 31.57 (6C, β_{out}), 22.71 (12C, γ_{in}), 21.85 (6C, γ_{out}), 13.78 (6C, δ_{out}), and 14.37 (12C, δ_{in}).

$Au_{25}(SBu)_{18}^0$. ^{1}H NMR: 25.0 (very br s, 24H, α_{in}), 5.067 (m, 12H, α_{out}), 3.484 (br m, 24H, β_{in}), 1.739 (m, 12H, β_{out}), 2.562 (m, 24H, γ_{in}), 1.561 (m, 12H, γ_{out}), 1.595 (br t, 36H, δ_{in}), 0.779 (t, 18H, δ_{out}). ^{13}C NMR: 38.3 (6C, α_{out}), 45.03 (6C, β_{out}), 31.09 (12C, γ_{in}), 23.3 (6C, γ_{out}), 17.19 (12C, δ_{in}), and 14.75 (6C, δ_{out}).

$Au_{25}(SMePr)_{18}$

[*n*-Oct_4N^+][$Au_{25}(SMePr)_{18}^-$]. ^{1}H NMR: 3.840 (br s, 24H, α_{in}), 3.084 (d, 12H, α_{out}), 2.387 (12H, sept, β_{in}), 2.156 (6H, sept, β_{out}), 1.353 (72H, d, γ_{in}), 1.113 (36H, d, γ_{out}). ^{13}C NMR: 46.6 (6C, α_{in}), 42.6 (6C, α_{out}), 34.5 (12C, β_{in}), 33.2 (6C, β_{out}), 22.6 (24C, γ_{in}), 22.1 (12C, γ_{out}).

$Au_{25}(SMePr)_{18}^0$. ^{1}H NMR: 14.39 (very br s, 24H, α_{in}), 4.973 (br s, 12H, α_{out}), 2.24 (12H, sept, β_{in}), 1.856 (6H, sept, β_{out}), 2.31 (72H, broad s, γ_{in}), 1.151 (36H, d, γ_{out}). ^{13}C NMR: 44.01 (6C, α_{out}), 31.2 (6C, β_{out}), 22.1 (24C, γ_{in}), 15.2 (12C, γ_{out}).

5. Electrochemistry. The electrochemical experiments were carried out in DCM containing 0.1 M *n*-tetrabutylammonium hexafluorophosphate, under an Ar atmosphere in a glass cell thermostatted at 25 °C. The working electrode was a 0.0164 cm^2 glassy-carbon disk, the counter electrode was a Pt wire, and an Ag wire served as the quasi-reference electrode. The latter was then referenced against the KCl saturated calomel electrode, SCE. We used a CHI 660c electrochemical workstation. To minimize the ohmic drop between the working and the reference electrodes, we used the positive feedback correction. The experiments were conducted by cyclic voltammetry, using a 1 mM solution of the cluster. The peak current (i_p) measured at low scan rates (v) allowed determining the diffusion coefficient D by using the equation that relates $i_p/v^{1/2}$ to $D^{1/2}$.[53: R. S. Nicholson, I. Shain, Anal. Chem. 1964, 36, 706– 723.] The radius of the MPC (r_{MPC}) was calculated from D by using the Stokes–Einstein–Sutherland equation, $D = k_B T/6\pi\eta r_{MPC}$, where k_B is the Boltzmann constant and η is the solvent viscosity. In Figure S5, the D and the r_{MPC} values are compared with those, previously obtained,[S3] of $Au_{25}(SEt)_{18}$, $Au_{25}(SPr)_{18}$, and $Au_{25}(SBu)_{18}$.

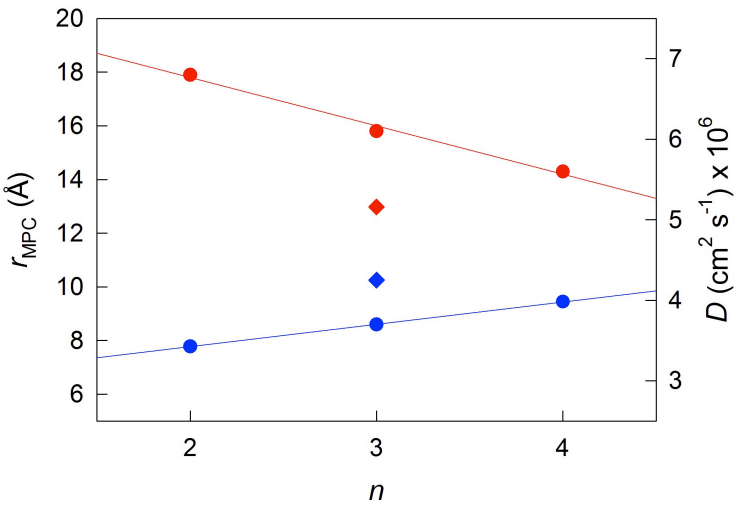

Figure S5. Dependence of the diffusion coefficient D (red circles, scale on right) and the MPC radius r_{MPC} (blue circles, scale on left) on the number of carbon atoms (n) forming the main ligand chain.

6. Simulation of the ENDOR Spectra. Figures S6-8 show the ENDOR spectra of $Au_{25}(SEt)_{18}^{0}$, $Au_{25}(SPr)_{18}^{0}$, and $Au_{25}(SMePr)_{18}^{0}$, together with the corresponding simulation, carried out as described in the main text.

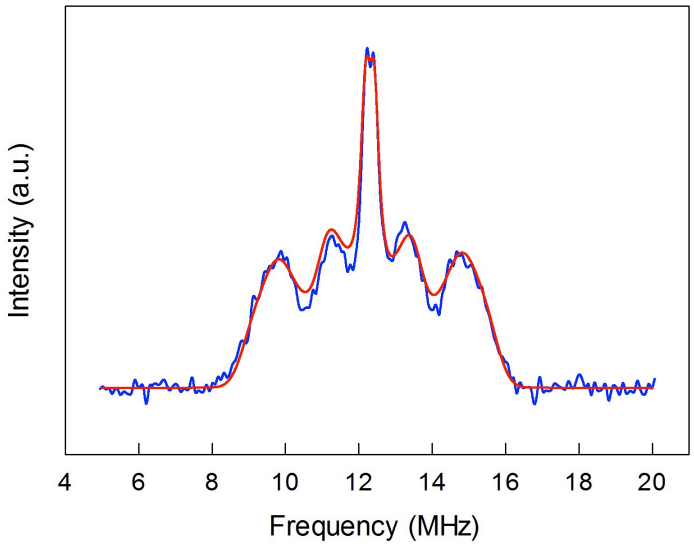

Figure S6. Baseline-corrected ^{1}H-ENDOR spectrum (blue) and simulation (red) for $Au_{25}(SEt)_{18}^{0}$ in toluene at 5 K.

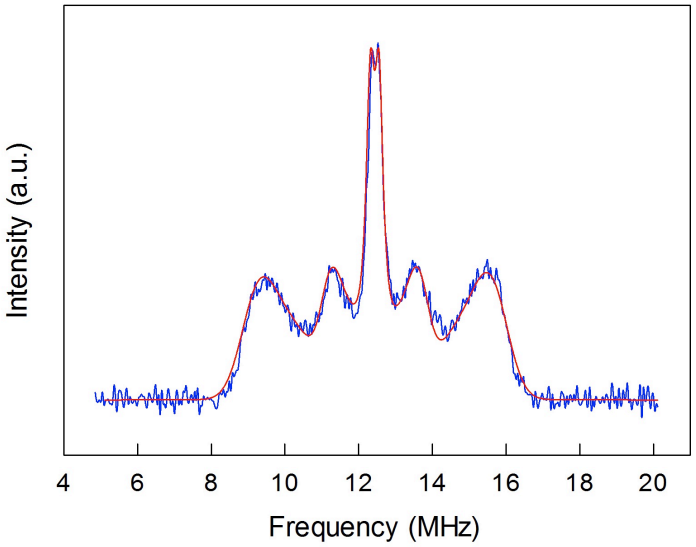

Figure S7. Baseline-corrected ^{1}H-ENDOR spectrum (blue) and simulation (red) for $Au_{25}(SPr)_{18}^{0}$ in toluene at 5 K.

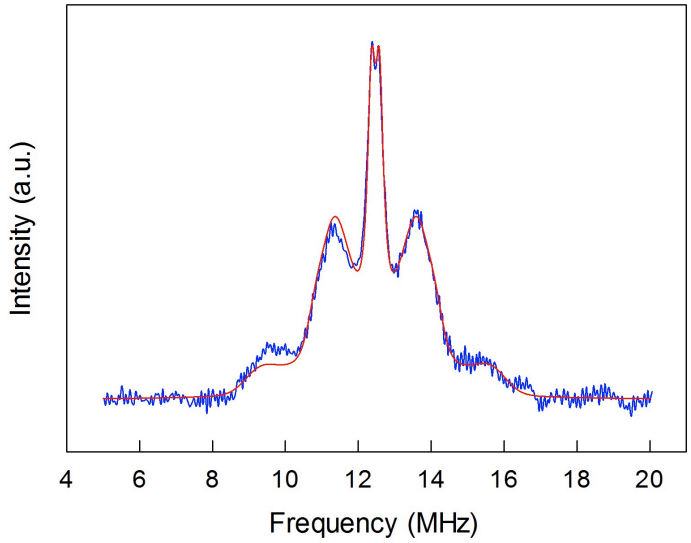

Figure S8 Baseline-corrected ^{1}H-ENDOR spectrum (blue) and simulation (red) for $Au_{25}(SMePr)_{18}^{0}$ in toluene at 5 K.

7. X-ray Crystallography. Crystallographic data for $Au_{25}(SPr)_{18}^{0}$ were collected at 170 K with Mo *K*α radiation (λ = 0.71073 Å) by using an Agilent SuperNova diffractometer equipped with Atlas CCD area detector. For data measurement and processing the CrysAlisPro software[S4] was employed. The intensities were corrected for absorption with analytical numeric absorption correction method[S5]. The structure was solved by direct methods[S6] integrated in the program of Olex2.[S7] Full-matrix least-squares refinements on F^2 were carried out using SHELXL-2015.[S8] Due to a very minor, yet significant on the gold atoms, around 95:5 positional disorder of the Au_{25} core was assigned. The SPr groups were not modeled accordingly but refined with full occupancy, yet they were constrained by "DFIX" and "ISOR" commands for reasonable geometry and thermal motion. In addition, one carbon atom (C2) in a SPr group in the asymmetric unit was found to be disordered over two sites and the two positions of the C2 atom (ratio 0.68:0.32) atom were constrained to have the same anisotropic thermal motion. The

H atoms were calculated to their idealized positions with constrainted isotropic thermal factors (1.2 or 1.5 times of U_{eq}(C)) and refined as riding atoms. Crystal data for $Au_{25}(SPr)_{18}^0$: black plates, 0.0144 × 0.0405 × 0.0619 mm, FW = 6276.78, $C_{54}H_{126}Au_{25}S_{18}$, trigonal, space group R-3, a = 16.771(2) Å, b = 17.771(2) Å, c = 27.217(2) Å, α = 90°, β = 90°, γ = 120°, V = 7444(2) Å^3, Z = 3, D_c = 4.201 g/cm^3, F(000) = 8139, μ = 37.189 mm^{-1}, T = 170.00(10) K, $2\theta_{max}$ = 56.0°, 3240 reflections, 2181 with $I_o > 2\sigma(I_o)$, R_{int} = 0.0346, 190 parameters, 68 restraints, GoF = 0.986, R_1 = 0.0474 [$I_o > 2\sigma(I_o)$], wR_2 = 0.0935 (all reflections), -2.034 < Δρ < 1.608 e/Å^3. The structure has been deposited to the Cambridge Crystallographic Data Centre with CCDC number 1453036, and the data can be obtained free of charge *via* www.ccdc.cam.ac.uk/data_request/cif.

8. DFT Calculations. *Ab initio* MD was carried out at the Density Functional Theory level using the generalized gradient approximation (GGA) and the PBE exchange-correlation functional. LANL2DZ (19 valence electrons) was employed for Au atoms, and the D90 basis set was used for (S, C, and H). All calculations were carried out with the program Gaussian 09, revision E.01.[S9]

9. References

S1. T. Dainese, S. Antonello, J. A. Gascón, F. Pan, N. V. Perera, M. Ruzzi, A. Venzo, A. Zoleo, K. Rissanen and F. Maran, *ACS Nano*, 2014, **8**, 3904-3912.

S2. A. Venzo, S. Antonello, J. A. Gascón, I. Guryanov, R. D. Leapman, N. V. Perera, A. Sousa, M. Zamuner, A. Zanella and F. Maran, F., *Anal. Chem.*, 2011, **83**, 6355-6362.

S3. S. Antonello, T. Dainese, M. De Nardi, L. Perotti and F. Maran, *ChemElectroChem.*, 2016, **3**, 1237-1244.

S4. CrysAlisPro, version 1.171.37.35; Agilent Technologies Ltd: Yarnton, England, 2014.

S5. R. C. Clark and J. S. Reid, *Acta Crystallogr.*, 1995, **A51**, 887–897.

S6. G. M. Sheldrick, *Acta Crystallogr.*, 2008, **A64**, 112–122.

S7. O. V. Dolomanov, L. J. Bourhis, R. J. Gildea, J. A. K. Howard and H. Puschmann, *J. Appl. Cryst.*, 2009, **42**, 339–341.

S8. G. M. Sheldrick, *Acta Crystallogr*., 2015, **C71**, 3-8.

S9. Gaussian 09, Revision E.01, M. J. Frisch, G. W. Trucks, H. B. Schlegel, G. E. Scuseria, M. A. Robb, J. R. Cheeseman, G. Scalmani, V. Barone, B. Mennucci, G. A. Petersson, H. Nakatsuji, M. Caricato, X. Li, H. P. Hratchian, A. F. Izmaylov, J. Bloino, G. Zheng, J. L. Sonnenberg, M. Hada, M. Ehara, K. Toyota, R. Fukuda, J. Hasegawa, M. Ishida, T. Nakajima, Y. Honda, O. Kitao, H. Nakai, T. Vreven, J. A. Montgomery, Jr., J. E. Peralta, F. Ogliaro, M. Bearpark, J. J. Heyd, E. Brothers, K. N. Kudin, V. N. Staroverov, R. Kobayashi, J. Normand, K. Raghavachari, A. Rendell, J. C. Burant, S. S. Iyengar, J. Tomasi, M. Cossi, N. Rega, J. M. Millam, M. Klene, J. E. Knox, J. B. Cross, V. Bakken, C. Adamo, J. Jaramillo, R. Gomperts, R. E. Stratmann, O. Yazyev, A. J. Austin, R. Cammi, C. Pomelli, J. W. Ochterski, R. L. Martin, K. Morokuma, V. G. Zakrzewski, G. A. Voth, P. Salvador, J. J. Dannenberg, S. Dapprich, A. D. Daniels, Ö. Farkas, J. B. Foresman, J. V. Ortiz, J. Cioslowski, and D. J. Fox, Gaussian, Inc., Wallingford CT, 2009.